International Journal of Engineering & Technology, 7 (3.36) (2018) 101-107

International Journal of Engineering & Technology

Website: www.sciencepubco.com/index.php/IJET

Research paper

Plantain Peel Mediated Green Synthesis Iron Oxide Nanoparticles, Surface Functionalization, and Them Performance towards Methylene Blue and Methyl Orange Dye Removal

Woan Giun Tan[1], Wei Ming Ng[2], Jit Kang Lim[2], Hui Xin Che[1,2*]

[1] Faculty of Engineering and Built Environment, SEGi University, 47810, Selangor, Malaysia
[2] School of Chemical Engineering, Universiti Sains Malaysia, Nibong Tebal, Penang, 14300, Malaysia
** Corresponding author E-mail: chehuixin@segi.edu.my*

Abstract

Currently, green synthesis approach is used as the biocompatible, eco-friendly, and sustainable alternative of conventional approaches to synthesize iron oxide nanoparticles. In this work, magnetic iron oxide nanoparticles were synthesized by using plantain peel extract via green and biogenic approach. The surface of green synthesized iron oxide nanoparticles was functionalized to increase the stability of the nanoparticles and maintain the coexisting of both magnetic and catalytic property of the nanoparticles at the same time. Two kinds of surface functionalization structures were synthesized in this study, included silica core-iron oxide shell nanoparticles and silica core-PDDA polymerized iron oxide shell nanoparticles. The main concern of this study is the performance of bare and surface functionalized green synthesized nanoparticles. Methylene blue and methyl orange dyes were used as the model of dye removal test to indicate the feasibility of the synthesized nanocomposites. In summary, surface functionalized nanocomposites achieved higher dye removal efficiency than bare green synthesized iron oxide nanoparticles in both the methylene blue and methyl orange degradation test. Methylene blue dye was removed in higher rate than methyl orange dye due to the presence of negatively charged iron oxide nanoparticles with both the adsorptive and catalytic properties. At last, the components present in plantain peel extract were confirmed by using Fourier Transform Infrared Spectroscopy.

Keywords: *Dye removal; Green technology; Iron oxide nanoparticles; Plantain peel; Surface functionalization*

1. Introduction

Nanotechnology is a technology to manipulate matter through some chemical and/or physical processes to produce nanostructured materials with novel properties and functions [1]. In recent years, nanostructured materials are attracting great interest in different fields such as research and development [2], biomedical [3], storage media [4], and environmental remediation [5]. The properties that empower the application of nanomaterials in those fields are their sizes (diameter range between 1-100 nanometers) [6], magnetic properties [7], and catalytic properties [8]. Among the different types of nanostructured materials, much interest has been paid to iron oxide nanoparticles (FeONPs) due to their specific shape, size, morphology, and structure [9]. The conventional ways to synthesize FeONPs are pyrolysis and attrition method. However, some disadvantages associated with these methods are low yielding rate, high production cost, the formation of deficient surfaces, and high energy consumption [10]. As a result, chemical synthesis methods are exploited to synthesize FeONPs. The common ways to synthesize FeONPs chemically are co-precipitation [11], sol-gel method [12], microemulsion [13], thermal decomposition [14], and sonochemical synthesis [15]. Inevitably, there are also some drawbacks on it which are the adoption of toxic reducing agents such as sodium borohydride and hydrazine hydrate [16], and pollution caused by the iron precursor chemicals [10]. Therefore, research focus has shifted towards the exploitation of green synthesis FeONPs by clean and non-toxic synthesis protocols that minimize the usage of toxic chemicals to restore the environment [17].

In this case, the performance of green synthesized iron oxide NPs (G-FeONPs) plays an important role in showing that the green synthesis methods can be used as the alternative way to substitute the chemical synthesis method. Here, the G-FeONPs were synthesized by using plantain peel extracts (PPE) [18]. The G-FeONPs were studied to explore their catalytic and magnetic properties to be used for dye removal in wastewater remediation purpose. Two types of surface functionalized nanocomposites were synthesized, including the silica core-PDDA polymerized iron oxide shell (SCPPIS) nanocomposites and silica core-iron oxide shell (SCIS) nanocomposites. Whereby, layer-by-layer (LbL) technique was used to assemble the G-FeONPs into core-shell structure [19]. Both of the surface functionalized G-FeONPs were compared to each other and to the bare G-FeONPs in order to differentiate their features accordingly.The organic dyes, methylene blue (MB) and methyl orange (MO) were employed as the cationic and anionic dye in this work to compare their performance through dye removal test. The catalytic function of both bare and surface functionalized G-FeONPs can be observed and analyzed by Fenton reactions in the dye removal test [20]. In the Fenton system, hydroxyl radicals (OH•) with high oxidizing ability are generated by both of the Fenton's reaction (Fe^{2+}/H_2O_2) and Fenton-like reaction

(Fe^{3+}/H_2O_2) [8]. The OH• produced will attach to the organic dye pollutants (RH) and then generate organic intermediate (R•). At the end, the R• with lower molecular weight will be further decomposed until complete mineralization into water and carbon dioxide as the final products [21].

2. Experimental

2.1. Preparation of plantain peel extracts

The waste peels after consuming plantains were cleaned properly by using deionized water (DIW). The plantain peels were dried after cleaning under sunlight. The dried peels were cut into small pieces. Ten grams of plantain peels were measured and placed into 250 ml round bottom flask. An amount of 100 ml of DIW was added into the flask with peels and refluxed for 1 hour at 80 °C to get the PPE solution in brown colour. The PPE solution was filtered by using cheese cloth after the solution cooled down to room temperature. The filtered extract solution was stored in a clean beaker at -4°C for further use [18].

2.2. Synthesis of iron oxide nanoparticles using plantain peel extracts

An amount of 40 ml of PPE solution was prepared. Then, 2.16 g of Iron (III) chloride hexahydrate ($FeCl_3.6H_2O$) and 6.56 g of sodium acetate (NaAC) were added into the prepared extract solution. Following this, the mixture solution was stirred at 1100 rpm for 2 hours at 70 °C. The formation of FeONPs can be indicated by the black precipitate nanoparticles (NPs) which were collected by centrifuging at 10000 ×g for 1 hour. The collected product was washed by using ethanol three times and then washed by DIW one time. Later, the cleaned product was dried in an oven at 70 °C for 12 hours. At last, the dried NPs were stored in a covered vial for further experiments [18].

2.3. Synthesis of silica nanotemplate via Stöber process

In this process, ethanol, tetraethylorthosilicate (TEOS), and 25% ammonia were mixed in the volume ratio of 30:1:3. The resultant mixture was stirred at 375 rpm for 2 hours. After the solution changed to milky condition, the mixture was centrifuged to separate the silica colloids as sediments at 5000 ×g for 15 minutes. The sediments of silica colloids were cleaned with DIW for three times to remove unreacted residues. After cleaning, the silica colloids were suspended and stored in 1mM sodium chloride (NaCl) solution [22].

2.4. Synthesis of PDDA-modified silica nanoparticles

At first, 0.01 g/ml of cationic poly(diallyldimethylammonium chloride) (PDDA) solution was prepared to coat onto the anionic silica colloids. The PDDA solution was ultrasonicated for 1 hour to promote the dispersity of the polyelectrolyte solution. Simultaneously, 0.01 g/ml of silica suspension was also ultrasonicated for 1 hour. In order to ensure the maximum monolayer coverage of PDDA on silica nanotemplates, the prepared concentration of the PDDA solution needed to be at least 500 times excess of the estimated amount. Then, the silica suspension was added dropwise into the PDDA solution with a mass ratio of 1:7.5 under ultrasonication. After this, the beaker containing the PDDA-modified silica NPs solution was left overnight on an end-to-end rotator at 40 rpm to complete the attachment PDDA onto the silica nanotemplates. The resultant PDDA-modified silica NPs solution was centrifuged at 5000 ×g for 15 minutes to obtain the NPs as sediments. The resultant product was washed with DIW two times to remove the excess reactants before dispersing into 1 mM of NaCl [22].

2.5. Synthesis of silica core-PDDA polymerized iron oxide shell nanocomposites

An amount of 0.0157 g of dried G-FeONPs was measured and added into 500 ml of DIW in a beaker before dispersing in ultrasonicator for 30 minutes. After that, 1 ml of PDDA-modified silica NPs was added dropwise into the G-FeONPs solution under ultrasonication. The resulted solution was then transferred to the end-to-end rotator at 40 rpm for 1 day. After 1 day, the SCPPIS nanocomposites were collected by centrifugation at 10000 ×g for 10 minutes. Then, the excess supernatants were removed by washing the SCPPIS nanocomposites with DIW for two times and followed by dispersing the SCPPIS nanocomposites in 1mM of NaCl solution **[**22**]**.

2.6. Synthesis of silica core-iron oxide shell nanocomposites

An amount of 0.0157 g of dried G-FeONPs was measured and put into 500 ml of DIW in a 500 ml beaker. 1 M of hydrochloric acid (HCl) was added into the solution until the pH value changed to 3. The resultant solution was dispersed in ultrasonicator for 1 hour. At the same time, 0.01g/ml of silica suspension was also ultrasonicated for 1 hour. After this, the silica suspension was added dropwise into the solution under ultrasonication condition. The resultant solution was left on end-to-end rotary at 40 rpm for 1 day. After 1 day, the SCIS nanocomposites were collected by centrifugation and washed by DIW two times. The SCIS nanocomposites were then dispersed in the 1mM of NaCl solution.

2.7. Dye removal test

Before the decolourization test, 5 ppm MB and MO solution were prepared from the 20 ppm MB and MO stock solution. The dye removal test was performed by using different NPs synthesized at each stage, included bare G-FeONPs with and without addition of H_2O_2, silica NPs, PDDA-modified silica NPs, SCPPIS nanocomposites, and SCIS nanocomposites. In the experiment, 1ml of 0.0157 g/ml bare G-FeONPs solution, 0.01 g/ml silica suspension, and 0.01 g/ml PDDA-modified silica NPs solution were added into 9 ml of dye solutions. In the case with addition of H_2O_2, 1 ml of 0.0157 g/ml bare G-FeONPs, 1 ml of 0.01 g/ml SCPPIS, and 1ml of SCIS were added into the mixture solution of 8.5 ml dye solution and 0.5 ml 10% H_2O_2 solution. There was no pH control in all the tests. The centrifuge tubes with mixture solution of NPs and dye solution were placed on end-to-end rotator and rotated at 40 rpm. Subsequently, the dye concentrations in the solutions were measured by using UV-Vis spectrophotometer after 6 hours contacting time at maximum wavelength of 666 nm for MB and 480 nm for MO [23]. The dye removal efficiency can be calculated by using equation (1).

$$\eta = \frac{C_o - C_f}{C_o} \times 100\% \quad (1)$$

where η (%) is the dye removal efficiency, C_o is the initial dye concentration (ppm), and C_f is the dye concentration after reaction (ppm).

2.8. Characterization of synthesized nanoparticles and nanocomposites

Fourier-transform infrared (FTIR) spectroscopy was employed to identify the components in the PPE after synthesis process. Besides, dynamic light scattering (DLS) and zeta potential analysis were also used to check the size (hydrodynamic diameter) and surface charge of the synthesized NPs.

3. Results and Discussion

3.1. Characterization and observation

3.1.1. Synthesis and characterization of green synthesized iron oxide nanoparticles

According to Venkateswarlu et al. (2013), PPE extract solution with carbohydrate reducing agent can be used to synthesize FeONPs. This can be proved by all the characterization results in the study, included TEM, EDX, XRD, and FTIR analysis [18]. Besides, the formation of FeONPs can be indicated by the colour changed from brown to black after adding the iron precursor, $FeCl_3.6H_2O$ into the extract solution as shown in Figure 1. The following equation (2) and (3) are showing the process to form G-FeONPs [18]:

$$Fe^{3+} + 3\ H_2O \rightarrow Fe(OH)_3\downarrow + 3\ H^+ \quad (2)$$

$$Fe(OH)_3\downarrow + \text{carbohydrates} \rightarrow \text{G-FeONPs} + \text{carbonic acid} \quad (3)$$

As showed in equation (2), $FeCl_3.6H_2O$ is hydrolyzed into ferric hydroxide ($Fe(OH)_3$) precipitate and hydronium ions at 70 °C with NaAC as the catalyst. The equation (3) is showing the reduction process of $Fe(OH)_3$ precipitate by carbohydrate reducing agent to form G-FeONPs and carbonic acid [18].

(a)

(b)

Fig. 1: The color of the extract solution: (a) before adding $FeCl_3.6H_2O$, (b) after adding $FeCl_3.6H_2O$.

FTIR spectroscopy: After mixing PPE with $FeCl_3.6H_2O$, the solution was characterized by FTIR spectroscopy after synthesis process. Figure 2 reveals the FTIR spectrum of the mixture solution. According to the FTIR spectrum, the peak at 3224 cm^{-1} is assigned to the O-H stretching in polyphenols and those bands within the range of 1330-1420 cm^{-1} are ascribed to the O-H bending of C-OH group in polyphenols. The peaks appears at 1570 cm^{-1} is attributed to the carboxylic acid stretching in carbonic acid. The peaks located around 1048 cm^{-1} and 1021 cm^{-1} could be assigned to the C-O stretch in cellulose from the plantain peels. The presence of peak ≈ 920 cm^{-1} is attributed by the iron perturbation which indicated the presence of iron in the solution. The peak at 791 cm^{-1} is due to the presence of O-H stretching in goethite (α-FeOOH). The two peaks within the region of 630-660 cm^{-1} are typical absorption peaks of maghemite (γ-Fe_2O_3). From this result, the presence of magnetite (Fe_3O_4) can be confirmed by these two peaks as γ-Fe_2O_3 is the oxidation product of Fe_3O_4 [24].

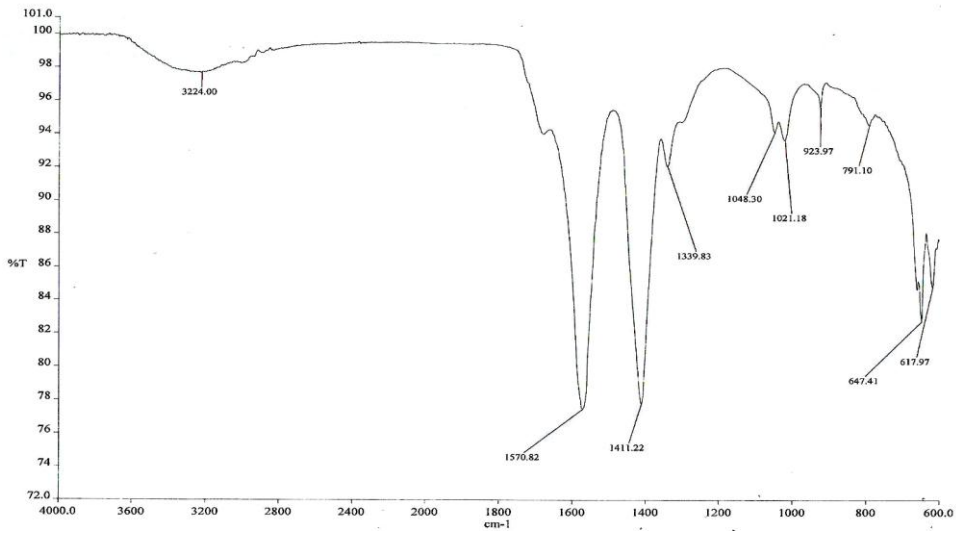

Fig. 2: FTIR spectrum of PPE solution after synthesis process.

Magnetic performance: The magnetic response of G-FeONPs was studied by using UV-Vis spectrophotometer with the maximum wavelength at 600 nm. An external magnetic bar was placed next to the vial containing G-FeONPs during the magnetic kinetic study. As demonstrating in the Figure 3, the absorbance was lower for the system in the presence of external magnetic field. Similarly important, the magnetic response of G-FeONPs can also be represented through another qualitative route as showed in Figure 4 in which the G-FeONPs can be successfully attracted or collected by the external magnet bar.

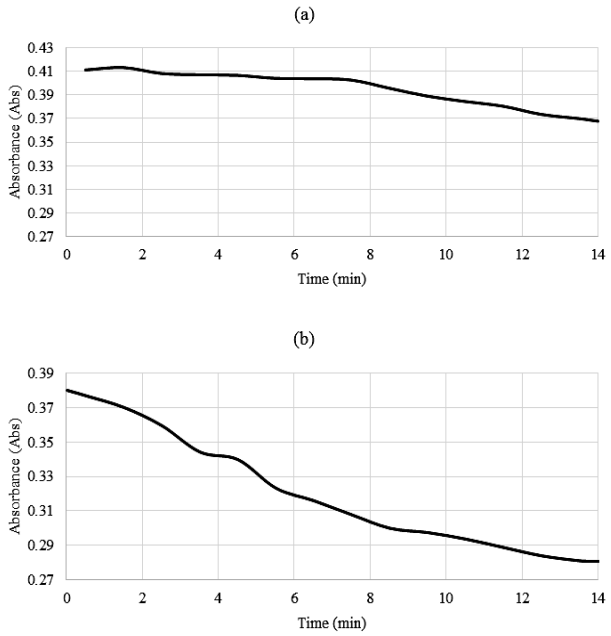

Fig. 3: The sedimentation loop of G-FeONPs: (a) without external magnetic field, (b) with external magnetic field.

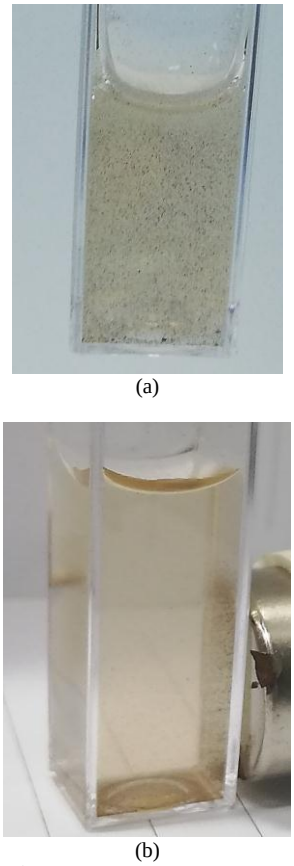

Fig. 4: The solution of G-FeONPs in the: (a) absence of magnetic bar, (b) presence of magnetic bar.

3.1.2. Synthesis of silica nanoparticles

Stöber process was employed to synthesize silica NPs in this work. During the process, the TEOS was first hydrolysed in ethanol and then followed by the condensation with ammonia [25]. Figure 5 is showing the formation of silica NPs solution with milky colour condition while Figure 6 is showing the silica NPs sediments after centrifuging the solution.

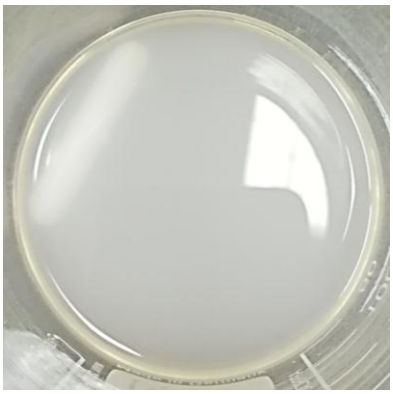

Fig. 5: Milky color silica colloids solution.

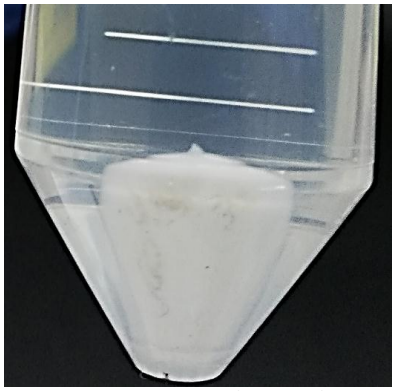

Fig. 6: Silica colloids sediment after centrifuging process.

3.1.3. Dynamic light scattering and zeta potential measurements

Malvern Zetasizer Nanoseries was used to perform DLS and zeta potential measurements in order to obtain the hydrodynamic diameter and surface charge of the synthesized NPs in this study [26]. The results obtained were summarized in Table 1 for different kinds of synthesized NPs.

Table 1: Hydrodynamic diameter and zeta potential of different types of NPs.

Sample of NPs	Hydrodynamic diameter (nm)	Zeta Potential (mV)
Silica NPs	225.50	-42.30
PDDA polymer solution	59.84	11.20
Cluster of G-FeONPs (neutral condition)	484.20	-32.80
Cluster of G-FeONPs (acidic condition)	484.20	+6.93
PDDA-modified silica NPs	334.60	+66.4
SCPPIS nanocomposites	398.80	+20.5
SCIS nanocomposites	310.50	-24.7

According to the zeta potential results, the surfaces of silica NPs and G-FeONPs are negatively charged. Therefore, there are two ways to coat the G-FeONPs onto the silica NPs for surface functionalization. The first method was utilizing positively charged PDDA polymer polyelectrolyte as the bridge between negatively charged silica NPs and G-FeONPs. In this case, LbL assembly technique was playing the main role in which the adsorption of oppositely charged particles took place to form SCPPIS nanocomposites. The silica NPs decorated with PDDA polyelectrolyte successfully reversed the surface charges of silica NPs from -42.30 mV to +66.4 mV. This positively charged PDDA-modified silica NPs facilitated the attachment of negatively charged G-FeONPs by electrostatic attraction forces. Following this, the SCPPIS nanocomposites were produced with a net zeta potential value of +20.5 mV. The presence of negatively charged G-FeONPs on the surfaces of PDDA-modified silica NPs was unable to reverse the

positively charged surfaces. Instead, the presence of G-FeONPs suppressed the zeta potential value from higher positively charges +66.4 mV to lower positively charges +20.5 mV. Besides, there was also an increase of the hydrodynamic diameter of PDDA-modified silica NPs from 334.6 nm to 398.8 nm after coating with G-FeONPs. These results validated the successful integration of G-FeONPs onto the PDDA-modified silica NPs, forming three-layer-composites.

On the other hand, the second method involved the modification of the surface charges on G-FeONPs in acidic condition. According to Yu and Chow (2004), the isoelectric point of bare FeONPs is around pH 7 [27]. By using this concept, the G-FeONPs were subjected into pH 3 acidic solution to shift the pH value across the isoelectric point in order to alter the zeta potential from negative value -32.8 mV to positive value +6.93 mV. Afterwards, the positively charged G-FeONPs can be coated onto negatively charged silica NPs to form SCIS nanocomposites without the need of bridging polymer. As indicating in the result, the zeta potential value was suppressed from -42.3 mV to -24.7 mV. The small change in the zeta potential value indicated that the low positively charged G-FeONPs were not sufficient to reverse the surface charge of silica NPs. Therefore, the bonds between silica NPs and G-FeONPs were not stable enough and possible to be disintegrated again. In like manner, the performance of SCIS nanocomposite in dye removal test may not completely dominated by the nanocomposites but also affected by the disintegrated silica NPs due to the unstable bonds.

Furthermore, the results obtained in the DLS analysis can also be used to indicate the occurrence of agglomeration of bare G-FeONPs. The hydrodynamic diameter of the surface functionalized SCPPIS nanocomposites and SCIS nanocomposites are 398.8 nm and 310.5 nm respectively after integrating G-FeONPs onto the PDDA-modified silica NPs and the silica nanotemplates. In contrast, the size of the agglomerated bare G-FeONPs is 484.2 nm which is obviously larger size than both of the surface functionalized nanocomposites. As a result, this validated that G-FeONPs are agglomerating in the absence of surface functionalization. Inevitably, the agglomeration condition was significantly affect the dye removal rate in this case.

3.2. Dye removal test

3.2.1. Methylene blue dye degradation

In dye removal experiment, silica NPs with highest negative zeta potential value, -42.3 mV possessed highest dye removal efficiency of 93.63 %. The silica NPs with negative charge can easily attract the cationic MB dye by electrostatic attraction force. This can be indicated by the change in the colour of silica NPs from milky colour to blue colour at the end of the experiment. However, decreasing in the dye removal efficiency of silica NPs can be observed after coating the surface of NPs with polycation PDDA. In this case, the negative zeta potential of silica NPs was reversed to positive value of +66.4 mV. Following this, electrostatic repulsion force was induced between the positively charged surface of PDDA-modified silica NPs and the cationic MB dye, and thus reduced the removal efficiency to 15.29%.

In order to investigate the catalytic property of bare G-FeONPs, the performances of bare G-FeONPs in the reaction condition with H_2O_2 and without H_2O_2 were compared. The removal efficiency of MB dye was 10.56% in the absence of H_2O_2, while the removal efficiency was 77.12% in the presence of H_2O_2. According to this, the catalytic property of bare G-FeONPs can be concluded by the increase in removal efficiency after adding the H_2O_2. Nevertheless, negatively charged G-FeONPs showed lowest removal efficiency in the absence of H_2O_2 after comparing to other positively charged decolourizing agents. This case was dominated by reduction in surface area available for adsorption process after the agglomeration of G-FeONPs as showed in Figure 7 [28]. Even though, the larger size agglomerated G-FeONPs are normally heavier than individual NPs and hence more susceptible to gravitational pulling [28]. Following this, the gravitational sedimentation phenomena can help to separate the agglomerated G-FeONPs from the solution in an easier and cheaper way without the application of low gradient magnetic separation after dye degradation tests.

Fig. 7: Agglomeration of G-FeONPs.

Afterwards, the bare G-FeONPs were further compared with SCIS NPs and SCPPIS NPs. Among them, SCIS NPs with zeta potential of -24.7 mV achieved highest removal efficiency of 93.57%. Although the bare G-FeONPs have higher negatively charged surface than SCIS NPs, but the increased in surface area of surface functionalized NPs enhanced the dye removal performance of the nanocomposites [29]. Regarding this, the agglomeration of bare G-FeONPs was clearly validated in the section 3.1.3. It is also interesting to note that the removal efficiency achieved by the silica colloids was similar to the removal efficiency of SCIS NPs. From this, the assumption about the presence of disintegrated silica NPs in the SCIS NPs solution can be verified. Different from this, lowest removal efficiency of 34.66% was showed by the positively charged SCPPIS NPs among three of the decolorizing agents due to the presence of electrostatic repulsion forces. Thus, the more positive charges on the surfaces, the stronger the electrostatic repulsion forces, and the lower the MB dye removal efficiency can be achieved.

Table 2: MB dye removal efficiencies by different dye decolourizing agents.

Decolourizing agent	Dye removal efficiency, η (%)
H_2O_2 solution	3.96
Silica NPs	93.63
PDDA-modified silica NPs	15.29
Bare G-FeONPs	10.56
Bare G-FeONPs with H_2O_2	77.12
SCIS NPs with H_2O_2	93.57
SCPPIS NPs with H_2O_2	34.66

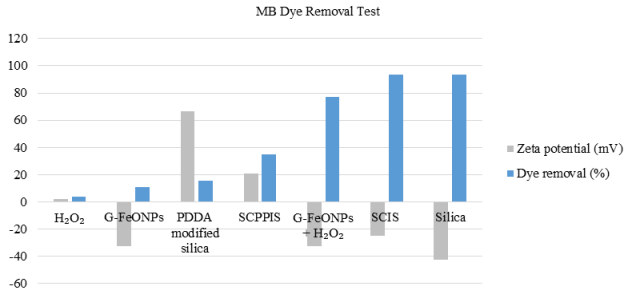

Fig. 8: Summary chart for the relationship between zeta potential values and dye removal efficiencies in MB dye removal test.

3.2.2. Methylene orange dye degradation

Before surface functionalization, bare G-FeONPs with H_2O_2 achieved highest dye removal efficiency of 47.66% in the presence of H_2O_2 after comparing to silica NPs, PDDA-modified silica NPs, and bare G-FeONPs without H_2O_2. Generally, the removal of anionic MO dye is more favourable by using a positively charged decolourizing agent. However, the negatively charged G-FeONPs with H_2O_2 showed better removal efficiency towards MO dye if

compared to positively charged PDDA-modified silica NPs. In this case, it can be proved that the bare G-FeONPs can degrade MO dye by utilizing both of the adsorption ability and catalytic property simultaneously during the decolourizing reaction [30]. Without the assistance of Fenton reaction between G-FeONPs and H_2O_2, the bare G-FeONPs can only adsorb 8.31% of the MO dye, which is obviously lower than the one with H_2O_2. On the other hand, the electrostatic repulsion forces were limiting the absorption of negatively charged MO dye molecules onto the similar charged surfaces of NPs, included silica NPs and G-FeONPs in the absence of H_2O_2.

After surface functionalization, positively charged SCPPIS NPs achieved 53.30% dye removal efficiency, which is more efficient than bare G-FeONPs. Comparing to the highly positively charged PDDA-modified silica NPs, SCCPIS NPs with lower positively charged surface showed higher efficiency. According to this result, the catalytic and adsorptive property of G-FeONPs were validated again. At the same time, the removal efficiency of SCPPIS NPs was also elevated by having the larger surface area which increased the chance of interaction between dye molecules and NPs after surface functionalization. In addition, the effectiveness in MO removal by SCPPIS NPs was also higher than the negatively charged SCIS NPs as the unfavourable path of electrostatic repulsion forces was dominated in dye degradation by SCIS NPs.

Table 3: MO dye removal efficiencies by different dye decolorizing agents.

Decolorizing agent	Dye removal efficiency, η (%)
H_2O_2 solution	12.80
Silica NPs	6.48
PDDA-modified silica NPs	24.62
Bare G-FeONPs	8.31
Bare G-FeONPs with H_2O_2	47.66
SCIS NPs with H_2O_2	17.24
SCPPIS NPs with H_2O_2	53.30

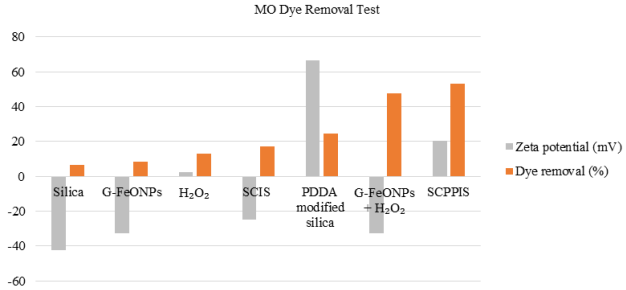

Fig. 9: Summary chart for the relationship between zeta potential values and dye removal efficiencies in MO dye removal test.

3.2.3. Comparison between the results of methylene blue and methyl orange dye degradation

The comparison between the results MB and MO dye degradation was summarized in Figure 10. As indicating in the results, the dye removal efficiency is strongly depending on the zeta potential value as depicted in Figure 10. Electrostatic attraction forces between oppositely charged surfaces are the main factor that contributes towards high dye removal efficiency [31]. As showed in the results, the MB dye degradation was accomplished with higher efficiency if compared to MO dye degradation. This scenario was primarily caused by the dominant decolourizing agent in this experiment, the negatively charged G-FeONPs with adsorptive and catalytic bifunctionalities, as the degradation of MB dye was more favourable in the presence of negatively charged surfaces.

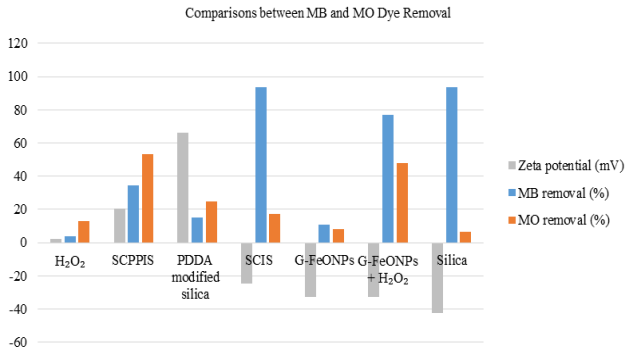

Fig. 10: Summary chart for the results of MB and MO dye removal test.

4. Conclusion and recommendations

G-FeONPs with magnetic and catalytic bifunctionalities can be readily synthesized by using PPE. After implementing surface functionalization, SCPPIS and SCIS nanocomposites achieved 53.30% and 93.57% in MO and MB dye degradation test respectively, which is higher than bare G-FeONPs in the presence of H_2O_2. In brief, the dye removal by FeONPs can benefit from the surface functionalization to minimize agglomeration phenomena, and thus surface area exposes to the dye molecules can be increased after that. At the same time, the surface functionalization method can also be employed to alter the charges on the surfaces of FeONPs depending on the circumstances required. However, the presence of bridging polymer between two layers of NPs is preferred to strengthen the bond and to avoid further disintegration. Last but not least, regeneration study is recommended in future studies to investigate the reusability of the G-FeONPs in related fields.

Acknowledgement

This work was supported by the SEGi Internal Research Fund [project number SEGiRF/2018-5/FoEBE-25/79].

References

[1] Environmental Protection Agency, *Nanotechnology white paper*, Science Policy Council, (2007), pp:4-21.

[2] Campos EA, Pinto DV, Oliveira JI, Mattos ED & Dutra RD (2015), Synthesis, Characterization and Applications of Iron Oxide Nanoparticles – a Short Review. *Journal of Aerospace Technology and Management* 7, 267-276.

[3] Mahdavi M, Ahmad MB, Haron MJ, Namvar F, Nadi B, Rahman MZ & Amin J (2013), Synthesis, Surface Modification and Characterisation of Biocompatible Magnetic Iron Oxide Nanoparticles for Biomedical Applications. *Molecules* 18, 7533-7548.

[4] Tartaj P, Morales MP, Gonzalez-Carreño T, Veintemillas-Verdaguer S & Serna CJ (2011), The Iron Oxides Strike Back: From Biomedical Applications to Energy Storage Devices and Photoelectrochemical Water Splitting. *Advanced Materials* 23, 5243-5249.

[5] Shipley HJ, Engates KE & Guettner AM (2011), Study of iron oxide nanoparticles in soil for remediation of arsenic. *Journal of Nanoparticle Research* 13, 2387-2397.

[6] Gogotsi Y, *Nanomaterials Handbook*, CRC Press, (2006), pp:1-4.

[7] Wu W, He Q & Jiang C (2008), Magnetic Iron Oxide Nanoparticles: Synthesis and Surface Functionalization Strategies. *Nanoscale Research Letter* 3, 397-415.

[8] Pereira MC, Oliveira LC & Murad E (2012), Iron oxide catalysts: Fenton and Fenton-like reactions–a review. *Clay minerals* 47, 285-302.

[9] Shojaee S & Mahdavi Shahri M (2016), Green synthesis and characterization of iron oxide magnetic nanoparticles using Shanghai White tea (Camelia sinensis) aqueous extract. *Journal of Chemical and Pharmaceutical Research* 8, 138-143.

[10] Herlekar M, Brave S & Kumar R (2014), Plant-Mediated Green Synthesis of Iron Nanoparticles. *Journal of Nanoparticles*, 1-9.
[11] Che HX, Yeap SP, Osman MS, Ahmad AL & Lim J (2014), Directed Assembly of Bifunctional Silica–Iron Oxide Nanocomposite with Open Shell Structure. *ACS Applied Materials & Interfaces* 6, 16508-16518.
[12] Kopanja L, Milosevic I, Panjan M, Damnjanovic V & Tadic M (2016), Sol–gel combustion synthesis, particle shape analysis and magnetic properties of hematite (α-Fe_2O_3) nanoparticles embedded in an amorphous silica matrix. *Applied Surface Science* 362, 380-386.
[13] Darbandi M, Stromberg F, Landers J, Reckers N, Sanyal B, Keune W & Wende H (2012), Nanoscale size effect on surface spin canting in iron oxide nanoparticles synthesized by the microemulsion method. *Journal of Physics D: Applied Physics* 45, 195001-195011.
[14] Gonzalez-Moragas L, Yu SM, Murillo-Cremaes N, Laromaine A & Roig A (2015), Scale-up synthesis of iron oxide nanoparticles by microwave-assisted thermal decomposition. *Chemical Engineering Journal* 281, 87-95.
[15] Hassanjani-Roshan A, Vaezi MR, Shokuhfar A & Rajabali Z (2011), Synthesis of iron oxide nanoparticles via sonochemical method and their characterization. *Particuology* 9, 95-99.
[16] Saif S, Tahir A & Chen Y (2016), Green Synthesis of Iron Nanoparticles and Their Environmental Applications and Implications. *Nanomaterials* 6, 1-26.
[17] Mahdavi M, Namvar F, Ahmad MB & Mohamad R (2013), Green Biosynthesis and Characterization of Magnetic Iron Oxide (Fe_3O_4) Nanoparticles Using Seaweed (Sargassum muticum) Aqueous Extract. *Molecules* 18, 5954-5964.
[18] Venkateswarlu S, Rao YS, Balaji T, Prathima B & Jyothi NV (2013), Biogenic synthesis of Fe_3O_4 magnetic nanoparticles using plantain peel extract. *Materials Letters* 100, 241-244.
[19] Che HX, Gwee SJ, Ng WM, Ahmad AL & Lim J (2018), Design of core-shell magnetic nanocomposite by using linear and branched polycation as an ad-layer: Influences of the structural and viscoelastic properties. *Colloids and Surfaces A: Physiochemical and Engineering Aspects* 539, 209-220.
[20] Shahwan T, Sirriah SA, Nairat M, Boyacı E, Eroğlu AE, Scott TB, Hallam KR (2011), Green synthesis of iron nanoparticles and their application as a Fenton-like catalyst for the degradation of aqueous cationic and anionic dyes. *Chemical Engineering Journal* 172, 258-266.
[21] Esteves BM, Rodrigues CSD & Madeira LM, *Applications of Advanced Oxidation Processes (AOPs) in Drinking Water Treatment*, Springer International Publishing, (2017), pp:211-255.
[22] Che HX, Yeap SP, Ahmad AL & Lim J (2014), Layer-by-layer assembly of iron oxide magnetic nanoparticles decorated silica colloid for water remediation. *Chemical Engineering Journal* 243, 68-78.
[23] Che H, Yeap S, Ahmad AL, Lim J (2014), Design and Synthesis Silica-polyelectrolyte-iron oxide Nanocomposite with Magnetic-Catalytic Bifunctionalities for Dye Removal. *Advanced Materials Research* 1024, 3-6.
[24] Laurent S, Forge D, Port M, Roch A, Robic C, Vander Elst L & Muller RN (2008), Magnetic Iron Oxide Nanoparticles: Synthesis, Stabilization, Vectorization, Physicochemical Characterizations, and Biological Applications. *Chemical Reviews* 108, 2064-2110.
[25] Nozawa K, Gailhanou H, Raison L, Panizza P, Ushiki H, Sellier E, Delville JP & Delville MH (2005), Smart Control of Monodisperse Stöber Silica Particles: Effect of Reactant Addition Rate on Growth Process. *Langmuir* 21, 1516-1523.
[26] Lim J, Yeap SP, Che HX & Low SC (2013), Characterization of magnetic nanoparticle by dynamic light scattering. *Nanoscale Research Letters* 8, 1-14.
[27] Yu S & Chow GM (2004), Carboxyl group (–CO_2H) functionalized ferrimagnetic iron oxide nanoparticles for potential bio-applications. *Journal of Materials Chemistry* 14, 2781-2786.
[28] Yeap SP, Lim J, Ooi BS & Ahmad AL (2017), Agglomeration, colloidal stability, and magnetic separation of magnetic nanoparticles: collective influences on environmental engineering applications. *Journal of Nanoparticles Research* 19, 368-383.
[29] Cipolatti EP, Silva MJ, Klein M, Feddern V, Feltes MM, Oliveira JV, Ninow JL & de Oliveira D (2014), Current status and trends in enzymatic nanoimmobilization. *Journal of Molecular Catalysis B: Enzymatic* 99, 56-67.
[30] Zhou L, He B & Huang J (2013), One-Step Synthesis of Robust Amine- and Vinyl-Capped Magnetic Iron Oxide Nanoparticles for Polymer Grafting, Dye Adsorption, and Catalysis. *ACS Applied Materials & Interfaces* 5, 8678-8685.
[31] Che H, Gwee S, Ahmad AL & Lim J (2015), Guided Assembly of Magnetic Nanocomposite with Open Shell Structure for Water Remediation. *Chemical Engineering Transactions* 45, 1489-1494.